

Gas shale hydraulic fracturing: a numerical investigation of the fracturing network evolution in the Silurian Longmaxi formation in the southeast of Sichuan Basin, China, using a coupled FSD approach

Y. Wang¹ · X. Li¹ · Y. X. Zhang¹ · Y. S. Wu¹ · B. Zheng¹

Received: 14 October 2015 / Accepted: 2 May 2016 / Published online: 21 July 2016
© Springer-Verlag Berlin Heidelberg 2016

Abstract This paper presents state-of-the-art modeling of complex hydraulic fracture network evolution in a naturally fractured formation with pre-existing bedding and cross joints, in the Silurian Longmaxi formation, southeast of Sichuan Basin, China. A flow-stress-damage coupling approach has been used in an initial attempt toward how reservoir responds to perforation angle, injection rate, in situ stress, cohesive and frictional strength of natural fractures. A detailed sensitivity study reveals a number of interesting observations resulting from these parameters on the fracturing network evolution in naturally fractured system. When the perforation angle is 60°, it gets to the maximum stimulated reservoir area (SRA). Injection rate as an operator parameter, it strongly impacts the interaction between hydraulic fractures and natural fractures, and associated SRA. In addition, in isotropic in situ stress field, fracturing effectiveness is not the best, complexity of SRA is enhanced when pre-existing fractures are oriented at an angle to the maximum stress. Moreover, the morphology of fracturing network and SRA is closely related to the frictional and cohesive strength of natural fractures. This work strongly links the production technology, geomechanical evaluation and aids in the understanding and optimization of hydraulic fracturing simulations in naturally fractured reservoirs.

Keywords Stimulated reservoir area (SRA) · Hydraulic fracturing · Fracturing network · Numerical simulation

Introduction

In shale gas reservoirs, the ultralow permeability of the reservoirs characteristic requires a large fracture network to maximize well performance. Hydraulic fracturing by stimulated reservoir volume (SRV) has made it possible for commercial production of shale gas by means of multistage fracturing of horizontal wells (Mayerhofer et al. 2008; Britt and Schoeffler 2009; King 2010; Wang et al. 2015a). The in-depth understanding of fracture network evolution mechanism in shale with stimulated reservoir volume can contribute to guiding the design of fracturing operation, controlling the morphology of fracture network of shale with SRV, thus improving the single well production of shale gas. Microseismic fracture mapping has shown that large fracture networks can be generated in many shale reservoirs. It is widely speculated that the stimulated natural fractures can make a significant contribution to the stimulated reservoir volume. The key to stimulated reservoir volume is the presence of natural fractures (Palmer and Moschovidis 2010; Cipolla et al. 2009a, b; Rahman and Rahman 2013; Wang et al. 2015b) and planes of weakness that can result in complex fracture geometries during stimulations. Many shale outcrops, cores and image logs contain fractures or fracture traces, and microseismic event patterns associated with hydraulic fracture stimulation have been ascribed to natural fracture reactivation. Natural features controlling SRV in shales include shale thickness, stress field and magnitude, presence of pre-existing natural open or healed natural fractures (e.g., sedimentary bedding fracture, interbedded fracture, shearing

This article is part of a Topical Collection in Environmental Earth Sciences on “Subsurface Energy Storage”, guest edited by Sebastian Bauer, Andreas Dahmke, and Olaf Kolditz.

✉ X. Li
lixiao@mail.iggcas.ac.cn

¹ Key Laboratory of Shale Gas and Geoenvironment, Institute of Geology and Geophysics, Chinese Academy of Sciences, Beijing 100029, China

fracture, tension-shearing fracture, decollement fracture, random fractures, etc.). While these parameters are not under direct human control, it is critical to understand how they will impact well results, completions and SRV effectiveness. In addition, the morphology of fracture network can also be affected by the fracturing operation factors (perforation angle, injection rate, the spacing between fracturing segments) and fracturing techniques (horizontal well multistage fracturing, synchronous fracturing, zipper fracturing and refracturing).

The hydraulic fracturing effectiveness evaluation based on both the fracture mechanics and material strength approaches can provide a general understanding of hydraulic fracturing, but analytical solutions are available for just a few simplified situations with the assumption of homogeneity (Jaeger and Cook 1969; Bruno and Nakagawa 1991) and only for single or multiple parallel fractures (Jeffrey et al. 2010; Nagel et al. 2013). In addition, for a hydraulic fracturing simulation experiment, it is not easy to quantitatively control the process of hydraulic fracture initiation and propagation, and it is difficult to measure the change of the pore pressure gradient field, due to fracture evolution in heterogeneous rock (Haimson 1968; Bredehoeft et al. 1976; Lockner and Byerlee 1977; Zoback et al. 1997; House 1987; Bruno and Nakagawa 1991). Moreover, for laboratory experiments, it is not easy to quantitatively control the cohesive and frictional parameters of natural fractures. For more complicated problems, such as the initiation and propagation of multiple natural fractures studied in this paper, the numerical modeling techniques can provide a feasible alternative solution. The numerical tools used to simulate the naturally fractured formations could be roughly divided into three kinds. The first kind is the traditional finite element approach (e.g., Rutqvist et al. 2002; Nassir et al. 2010). The second kind consists of simplified models based upon existing pseudo-3D models (Meyer and Bazan 2011) or simplified rule-based analytical models for addressing the complex interactions between a created hydraulic fracture and a natural fracture system (Kresse et al. 2011). In the third kind, the authors have developed and applied the discrete element model in capturing the fundamental hydromechanical behavior of hydraulic fracturing in naturally fractured reservoir (Al-Busaidi et al. 2005; Fu et al. 2013; Nagel et al. 2013). In the model, they highlighted the impact of fluid compressibility on hydraulic fracture geometry (a very compressible fluid created a more complex fracture geometry).

More importantly, in shale fracturing, one of the challenges for numerical models that influence the stimulation and productivity prediction is the heterogeneity of reservoirs. Firstly, the rock matrix is composed of many different kinds of mineral, crystal grain, pores and microcracks, etc. from the perspective of mesoscopic.

Secondly, the natural fractures are greatly developed in natural reservoirs from macroperspective. The massive multistage hydraulic fracturing used in shale stimulation results in a large number of fractures propagating simultaneously or sequentially. The naturally fractured formations under hydraulic loading exhibit a unique feature: The flow and the transport behaviors within developing fractures are dramatically different from those in rocks with existing fractures under the same loading. The permeability of rocks with existing fractures does not change, but it can change dramatically due to damage evolution in fracturing rocks. The influence of damage on the variation of permeability as well as the original nature of the existing fractures in reservoirs is critical to shear stimulation of natural fractures. Another major problem in characterizing the hydraulic behavior of reservoirs concerns the irregular flow paths that depend on the mechanical heterogeneity of the formations. In working with heterogeneous rocks, a key factor is to determine the specific data (e.g., compressive strength, elastic modulus, etc.) that are needed to ascertain the effect of heterogeneity on the complicated flow paths in fracturing formations. To solve the coupled flow-damage problems, Tang et al. (2002) proposed a flow-stress-damage (FSD) coupling model by taking into account the growth of existing fractures and the formation of new fractures. This FSD model can be used to trace the development of fractures and the associated fluid flow, and to simulate the overall response of rock masses arising from the fracture process under hydraulic and boundary loadings. This FSD model is different from the finite element modeling and distinct element modeling. The most unique feature of this code, which makes it totally different from other kind of numerical methods, is that it is based on the damage mechanics and finite element method, and the heterogeneity in the properties of rock is also considered (Tang et al. 2002; Wang et al. 2015a, b). In the model, the initiation and propagation of natural fractures are dynamic, not static, and the interaction behaviors (cross, offset and capture) of hydraulic fracture and natural fracture are automatically accomplished according to the mechanical characteristics.

In this paper, a discussion of discrete fracture network (DFN) generation and how it influences the hydraulic fracturing effectiveness is presented. Currently, few reports have been published to explore the effect of perforation angle on hydraulic fracturing. In this work, the hydraulic fracturing model was established to consider the macroscopic heterogeneity characteristic and microscopic heterogeneity characteristic simultaneously for a fractured shale gas reservoir, southeast Sichuan basin, China. Firstly, the fracture network evolution characteristics with different perforation angle (PA) are discussed so as to determine the optimal perforation angle that yields the maximum SRA.

Secondly, the parameter sensitivity analysis is conducted as a function of injection rate (IR), the in situ stress ratio (SR), cohesion (C) and internal frictional angle (IFA) of natural fractures. A sensitivity study reveals a number of interesting observations resulting from these parameters on the interaction between hydraulic fractures and natural fractures, the effectiveness of hydraulic fracturing.

Brief description of numerical model

RFPA-Flow code developed by Tang et al. (2002) is a numerical simulation tool using finite element analysis to handle the progressive failure of heterogeneous, permeable rock. Clearly, the model approaches contain a large number of assumptions and simplifications that can only be justified by comparing the model to experimental hydrofracturing data (Al-Busaidi et al. 2005). In this work, the coupled effects of flow, stress and damage on the extension of existing/new fractures and the permeability change due to damage evolution of the rocks were addressed. This coupled flow, stresses and damage (FSD) model in RFPA-Flow has been validated in the previous publications (Tang et al. 2002; Li et al. 2013; Wang et al. 2015a, b, 2016). Some assumptions of the code include: (1) The flow of the fluid is governed by Biot’s consolidation theory. (2) The rock is assumed to be brittle–elastic material with residual strength, and its loading and unloading behavior is described by elastic damage mechanics. (3) An element is considered to have failed in the tension mode when its minimum principal stress exceeds the tensile strength of the element, and to have failed in the shear mode when the shear stress satisfies the strength criterion defined by the Mohr–Coulomb failure envelope. (4) The permeability varies as functions of the stress states in elastic deformation, and increases dramatically when the element fails. (5) The local heterogeneity in the properties of rock masses is defined by Weibull function. By extending Biot’s theory (Biot 1941) to include the effects of stress on permeability, the basic formations of the analysis are:

$$\text{Equilibrium equation: } \frac{\partial \sigma_{ij}}{\partial x_{ij}} + \rho X_j = 0 \quad (i, j = 1, 2, 3) \tag{1}$$

$$\text{Strain - displacement equation: } \varepsilon_{ij} = \frac{1}{2} (\mu_{i,j} + \mu_{j,i}) \tag{2}$$

$$\varepsilon_v = \varepsilon_{11} + \varepsilon_{22} + \varepsilon_{33}$$

$$\text{Constitutive equation: } \sigma'_{ij} = \sigma_{ij} - \alpha p \delta_{ij} = \lambda \delta_{ij} \varepsilon_v + 2G \varepsilon_{ij} \tag{3}$$

$$\text{Fluid flow equation: } k \nabla^2 p = \frac{1}{Q} \frac{\partial p}{\partial t} - \alpha \frac{\partial \varepsilon_v}{\partial t} \tag{4}$$

$$\text{Coupling equation: } k(\sigma, p) = \xi k_0 \exp \left[-\beta \left(\frac{\sigma_{ii}/3 - p}{H} \right) \right] \tag{5}$$

where σ is stress; ρ is density; u is displacement; e is strain; X is component of body force; α is coefficient of pore water pressure; λ is Lamé coefficient; p is pore water pressure; δ is Kronecker constant; G is shear modulus; Q is Biot’s constant; k is coefficient of permeability; k_0 = initial coefficient of permeability; β is a coupling parameter that reflects the influence of stress on the coefficient of permeability; and $\xi (>1)$ is a mutation coefficient of permeability to account for the increase in permeability of the material during fracture formation. Equations (1)–(4) are based on Biot’s theory of consolidation (Biot 1941), and Eq. (5) represents the effect of stress on permeability, which is introduced to describe the dependency of permeability on stress and damage, and the relationship between permeability and stress is assumed to follow a negative exponential function.

When the stress of the element satisfies the strength criterion (such as the Coulomb criterion, Jaeger and Cook 1969), the element begins to fail. In elastic damage mechanics, the elastic modulus of the element may degrade gradually as damage progresses, and the elastic modulus of the damaged element is defined as follows:

$$E = (1 - D)E_0 \tag{6}$$

where D is the damage variable, E and E_0 are elasticity modulus of the damaged and the undamaged material, respectively.

When the tensile stress in an element reaches its tensile strength f'_{t} , the constitutive relationship illustrated in Fig. 3a is adopted. This is

$$\sigma'_3 \leq -f'_{t0} \tag{7}$$

The damage variable can be described by Tang et al. (2002) as:

$$D = \begin{cases} 0 & \bar{\varepsilon} \leq \varepsilon_{t0} \\ 1 - \frac{f'_{tr}}{E_0 \bar{\varepsilon}} & \varepsilon_{t0} \leq \bar{\varepsilon} \leq \varepsilon_{tu} \\ 1 & \bar{\varepsilon} > \varepsilon_{tu} \end{cases} \tag{8}$$

where f'_{tr} is the residual tensile strength of the element, and $\bar{\varepsilon}$ is equivalent principal strain of the element, ε_{t0} is the strain at the elastic limit, or threshold strain, and ε_{tu} is the ultimate tensile strain of the element at which the element would be completely damaged, as shown in Fig. 1a.

In this case the permeability can be described as:

$$k = \begin{cases} k_0 \exp[-\beta(\sigma'_3 - \alpha p)] & D = 0 \\ \xi k_0 \exp[-\beta(\sigma'_3 - \alpha p)] & 0 < D \leq 1 \end{cases} \tag{9}$$

where ξ ($\xi > 1$) is the damage factor of permeability, which reflects the damage-induced permeability increase

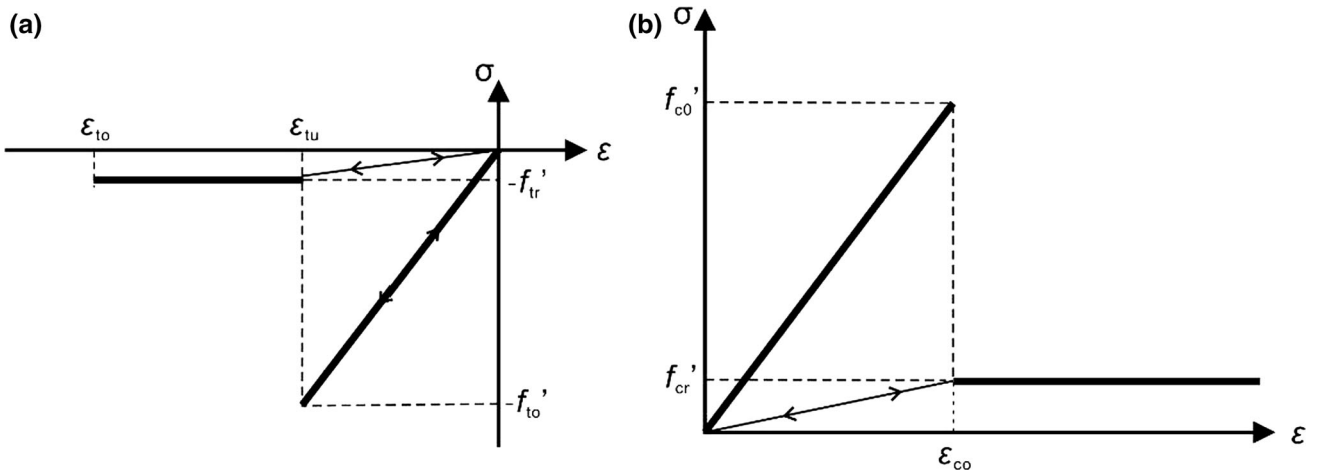


Fig. 1 Elastic–brittle damage constitutive law of element subject to uniaxial stress **a** the case under uniaxial tensile stress; **b** the case under uniaxial compressive stress)

(Tang et al. 2002). The value of ξ can be obtained from experimental tests (Thallak et al. 1991; Noghabai 1999).

In the model, both tensile and shear failure modes are considered. An element is considered to have failed in the tension mode when its minor principal stress exceeds the tensile strength of the element, as described by Eq. (6), and have failed in shear mode when the compressive or shear stress has satisfied the Mohr–Coulomb failure criterion (Fig. 1b) given by Tang et al. (2002):

$$F = \sigma'_1 - \sigma'_3 \frac{1 + \sin \phi'}{1 - \sin \phi'} \geq f'_{c0} \quad (10)$$

where σ'_1 is the major effective principal stress, σ'_3 is the minor effective principal stress, ϕ' is the minor effective angle of friction, f'_t is the tensile failure strength of the element, and f'_c is the compressive failure strength of the element. The damage factor under uniaxial compression is described as:

$$D = \begin{cases} 0 & \bar{\varepsilon} < \varepsilon_{cu} \\ 1 - \frac{f'_{cr}}{E_0 \varepsilon} & \bar{\varepsilon} \geq \varepsilon_{cu} \end{cases} \quad (11)$$

where f'_{cr} is the residual compressive strength, ε_{cu} is the ultimate compressive strain of the element at which the element would be completely damaged. In this case, the permeability can be described by

$$k = \begin{cases} k_0 \exp[-\beta(\sigma'_1 - \alpha p)] & D = 0 \\ \xi k_0 \exp[-\beta(\sigma'_1 - \alpha p)] & D > 0 \end{cases} \quad (12)$$

In RFPA-Flow, the specified loading is applied to the specimen incrementally in a quasi-static manner, and a flowchart outlining the pertinent steps of the analysis is given in Fig. 2. Coupled fluid flow and stress analyses are performed. At each loading increment, the fluid flow and

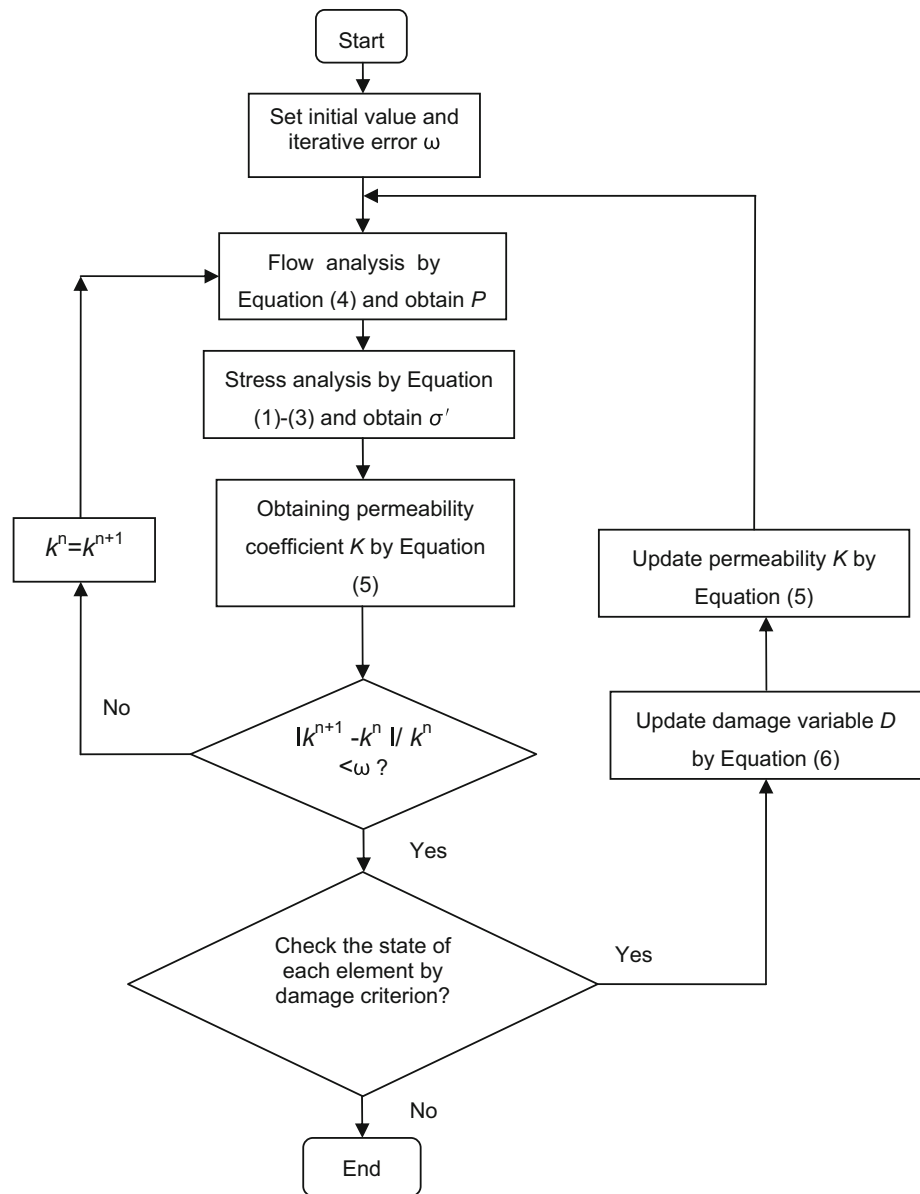
stress equations of the elements are solved and a coupling analysis is performed. The stress conditions of each element are then examined for failure before the next load increment is applied. If some elements are damaged in a particular step, their reduced elastic modulus and increased permeability at each stress or strain level are calculated using the above damage variable D as well as Eq. (6). Then, the calculation is restarted under the current boundary and loading conditions to redistribute the stresses in the specimen until no new damage occurs. Finally, the external load (or displacement) is increased and is used as input for the next step of the analysis. Therefore, the progressive failure process of a brittle material subjected to gradually increasing static loading can be simulated. A user-friendly pre- and post-processor is integrated in RFPA-Flow to prepare the input data and display the numerical results.

There are two features distinguishing RFPA-Flow from other numerical approaches: (1) by introducing heterogeneity of rock properties into the model, the RFPA-Flow code can simulate nonlinear deformation of a quasi-brittle behavior with an ideal brittle constitutive law for the local material;(2) by introducing a reduction of material parameters after element failure, the RFPA code can simulate strain-softening and discontinuous mechanics problems in a continuum mechanics mode. For heterogeneity, the material properties (failure strength σ_c and elastic modulus E_c) for elements are randomly distributed throughout the model by following a Weibull distribution:

$$\varphi = \frac{m}{\sigma_0} \left(\frac{\sigma}{\sigma_0}\right)^{m-1} \exp\left[-\left(\frac{\sigma}{\sigma_0}\right)^m\right] \quad (13)$$

where σ is the element strength and σ_0 is the mean strength of the elements for the specimen. For an elastic modulus,

Fig. 2 Flowchart of the RFPA-Flow model, modified after Yang et al. (2004)



E , the same distribution is used. We define m as the homogeneity index of the rock (Tang et al. 2002). According to the definition, a larger m implies a more homogeneous material and vice versa.

Numerical model setup

Why DFN modeling?

There are several reasons why DFN models are particularly useful for describing complex hydraulic fracturing in low-permeability shale formations. In low and ultralow-permeability rock matrix of shale, individual fractures that are

in close proximity, but not touching, are not well connected hydraulically. As a result, fluid flow between locations is dependent on properties of the fracture network geometry. Connectivity can be highly unpredictable, with weak connections between two nearby locations, but strong connection between more distant locations (McCabe et al. 1983; Cacas et al. 1990; McClure and Horne 2013). In hydraulically stimulated, fractured, low matrix permeability reservoirs, production logs typically show that productivity can be highly variable along individual wells within the same rock unit (Dezayes et al. 2010; Miller et al. 2011). Discrete fracture models are better at describing this sort of highly channelized, unpredictable behavior. In addition, stress perturbation can be handled much more accurately

with a DFN (McClure and Horne 2013). The stresses caused by fracture opening or sliding are very heterogeneous spatially, and effects on neighboring fractures are dependent on their relative orientations and locations. Stresses caused by fracture deformation have major effects on the process of stimulation.

DFN model and realization

It is believed that characteristics of DFN have a critical effect on the response of naturally fractured reservoirs to fluid injection. Explicit representation of the DFN with realistic characteristics is thus important in the numerical modeling. DFNs often are characterized by some statistical parameters, among them, fracture orientation distribution, fracture spacing distribution, fracture length distribution and fracture persistence of each fracture set, etc. (Engelder and Lash 2008; Olson 2003, 2004; Wang et al. 2015b). The combinations of these statistical characteristics that describe the geometrical properties of a DFN defined by the macroscale connectivity and directional flow preference of the DFN, and thus, are essential for the fluid transport characterization of an unconventional reservoir. From the outcrop observations, most of natural fractures are normal to bedding, faults, bed-parallel fractures and compaction fabric. Natural fractures may terminate abruptly at bedding planes, stylolites, or they may gradually taper. In outcrop, most fractures are barren (joints), while a few contain mineral cements. The shale is more prone to faulting than to sustaining opening-mode fractures. According to the results of core data, well log and water injection test (Fig. 3), we developed the corresponding DFN model to represent the bedding and cross natural fractures. For this study, a Baecher DFN generator was developed that was capable of creating a fracture network that satisfied the assigned input statistical characteristics and allowed for the quantitative variation of the studied case. The Baecher model (Baecher et al. 1978) is a flexible algorithm that can generate intricate joint networks. In this model, joints are assumed to have finite trace lengths, which follow some statistical distribution. The centers of the joints are located in space according to a Poisson point process. The orientations of joints in a Baecher network can either vary according to an orientation distribution or be constant. The number of joints generated in a Baecher network is controlled by a joint intensity measure. In order to avoid boundary effects for a specified model region, the Baecher algorithm first enlarges the region before generating joints. After generating the joints according to the required joint intensity measure, the algorithm then clips the network with the original bounding region. Joints of the Baecher network generally terminate in intact rock. The main parameters for Baecher DFN model include the joint orientation, dip, dip direction, joint length and joint intensity. The Baecher DFN

model can be regenerated, using a new sampling of the random variables (e.g., joint orientation, joint length).

RFPA-flow model setup

According to the DFN generator mentioned above, Baecher DFN model was used to describe the natural fracture system of shale in the Silurian Longmaxi formation in the southeastern Sichuan Basin, China. The geological structure of the outcrop is composed of two joint sets; they are bedding joints and cross joints. According to the research results about the relationship between mean or medium joint spacing and layer thickness in layered rocks (Mandal et al. 1994; Sagy and Reches 2004), it was suggested that the saturation intensity ($D_s = h/d$) for realistic geological cases converges to the range of $D_s = 0.75\text{--}3.0$ (i.e., $d/h = 1/3\text{--}4/3$). Figure 4 shows the geometry and the setup of the simulation model. The dimensions of the fractures have been converted by similarity criterion. The model represents a 2D horizontal section of a reservoir with laboratory scale. In the model, the injection is through a vertical wellbore in the center of the model, and the injected fluid was imposed on the wellbore at constant rate. The whole model is composed of 40,000 (200×200) identical square elements with dimension of $400 \text{ mm} \times 400 \text{ mm}$. The diameter of the injection hole was 15 mm. As shown in Fig. 4, The bedding joint had a spacing of 15 mm with normal distribution, std, of 3 mm. The cross joint had a spacing of 25 mm with normal distribution and std, of 5 mm.

The input material mechanical parameters for the numerical model are based on the work by Heng et al. (2015) and Li et al. (2015), as shown in Table 1. A series of simulations were conducted to evaluate the influence of the various parameters on hydraulic fracturing effectiveness and the network evolution caused by an injection wellbore. For case “a–d”, four simulations with perforation angles 0° , 30° , 60° and 90° are studied. For case “c” (corresponding to the maximum SRA), it is selected to study the responses of multiple parameters on hydraulic fracturing effectiveness, and another six cases of numerical simulations are reported, labeled with “1–6”. For case c-1, the influence of the injection rate on hydraulic fracturing effectiveness was investigated, by adopting values for injection rate, $IR = 0.005, 0.01, 0.02$ and 0.05 ml/s , respectively. Case c-2 was performed to consider the effect of stress ratio (which is defined as the ratio of σ_H/σ_V on hydraulic fracturing), such as $SR = 0.5, 0.75, 0.9$ and 1 , respectively. For case c-3, the effect of internal friction angle of cross joint on hydraulic fracturing effectiveness was studied, by considering $IFA = 5^\circ, 10^\circ, 33^\circ$ and 50° , respectively. Case c-4 was performed to consider the effect of internal friction angle of bedding joint on fracture network evolution, such as $IFA = 5^\circ, 10^\circ, 33^\circ$ and 50° , respectively. Value of internal friction angle is the same to case c-3. For case c-5, the effect



Fig. 3 Outcrop of Silurian Longmaxi shale formation in the southeastern Sichuan Basin. The water injection test is used to seek the natural fractures. Two sets of orthorhombic natural fractures were

presented after water injection test. The rock blocks (processed into 400 mm × 400 mm) were sampled from Shizhu County, Chongqing, China

of cohesion of cross joint on hydraulic fracturing effectiveness was studied, by considering $C = 3, 9, 15$ and 20 MPa, respectively. Case c-6 was performed to consider the effect of cohesion of bedding joint on fracture network evaluation, by considering $C = 3, 9, 15$ and 20 MPa, and the same to case c-5. Figure 6 shows the relationship of stimulated reservoir area, pore pressure and injection step for the four perforation situations.

For the base simulator, the horizontal stress (σ_H) was 18 MPa and the vertical stress (σ_V) was 20 MPa. The slick-water treatment is selected during the simulations, and fluid rheology is 1 cp. It is noteworthy that the simulation model is based on laboratory scale, not field scale. The reason is that because of a too large-scale calculation for field scale model, the computation efficiency is extremely low. The connection between the field scale and laboratory scale is by similarity criterion (Clifton and Abou-sayed 1979; Liu et al. 2000).

In this paper, the RFPA-Flow numerical model will be used to investigate the effect of perforation angle, injection rate and geomechanical parameters on network evolution. In addition to qualitative evaluation of the simulation results, the model responses are compared in an index of

stimulated reservoir area, which is defined as the interaction area of hydraulic fractures and natural fractures that have experienced a fluid pressure increase due to injection. As there is no precise criterion for defining the interaction area, a criterion based on fracture pressure change was employed in this work. The interaction area of HF and natural fractures having a pore pressure increase of 10 MPa above the initial pore pressure was considered as the stimulated reservoir area.

Effect of perforation angle on fracturing network evolution

In conventional reservoirs and tight gas sands, single-plane-fracture half-length and conductivity are the key drivers for stimulation performance. To create large single hydraulic fractures, many scholars pointed out that the perforation holes should be parallel to the maximum principal stress and perpendicular to the minimum principal stress (EI Rabaa 1989; King 1989; Hallam and Last 1991; Pearson et al. 1992). Men et al. (2013) have also performed simulation tests to study the influence of

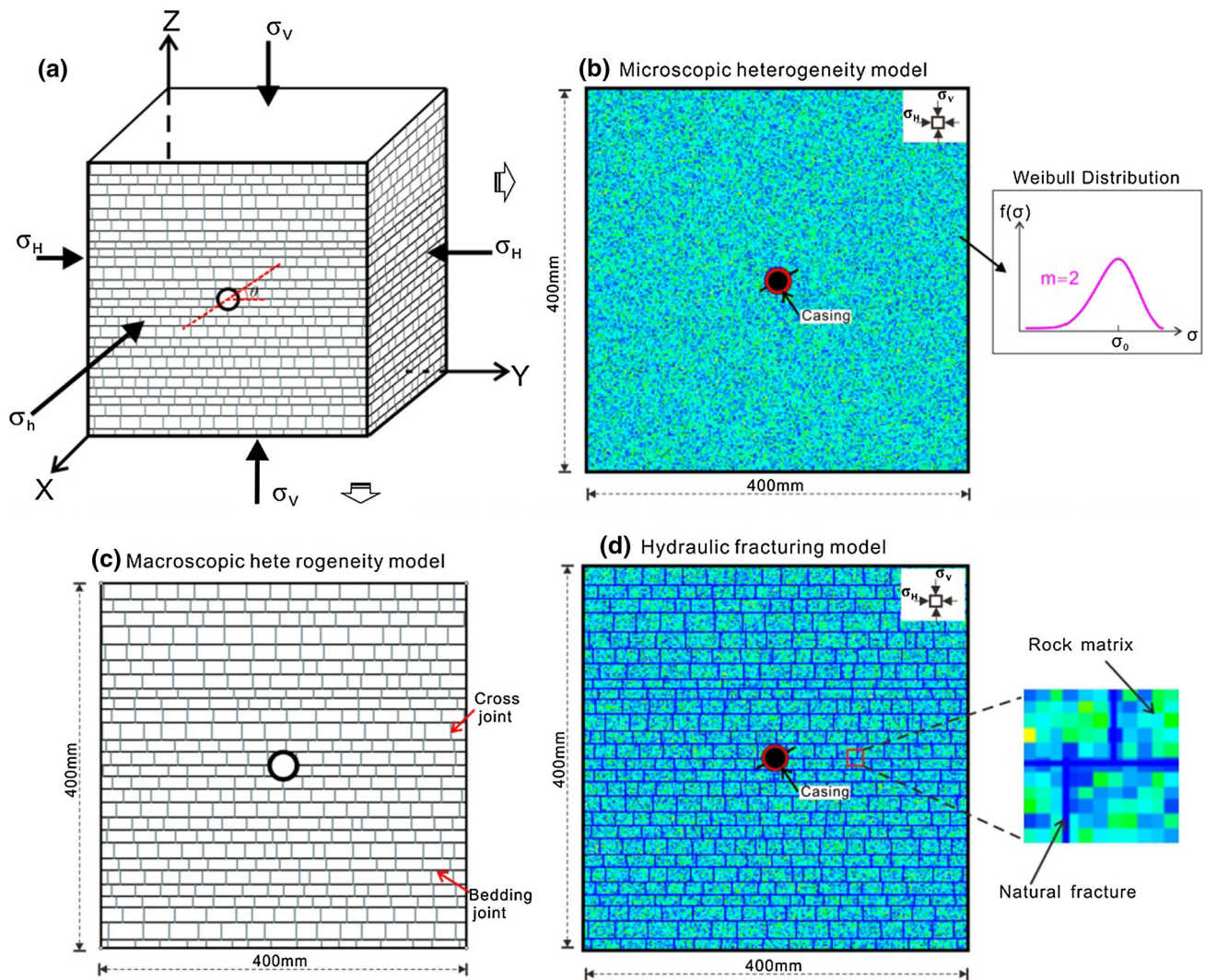


Fig. 4 Numerical model setup. **a** 3D simplified geological model of Silurian Longmaxi shale formation; **b** the microscopic heterogeneity background model, the failure strength and elastic modulus obey Weibull distribution; **c** the developed Beacher DFN mode, which

corresponds to macroscopic heterogeneity model. **d** The calculation model in this paper, considering the macroscopic and microscopic heterogeneity characteristics, simultaneously. Model “d” = model “b” +model “c”

Table 1 Input material mechanical parameters for the studied numerical model

Index	Rock matrix	Bedding joint	Cross joint	Unit
Homogeneity index (m)	2	1.8	1.8	
Elastic modulus (E_0)	60	30	30	GPa
Poisson’s ratio (ν)	0.25	0.3	0.3	
Internal friction angle (φ)	36	33	33	°
Cohesion (c)	16	9	9	
Compressive strength (σ_c)	450	150	120	MPa
Tensile strength (σ_t)	45	15	15	MPa
Coefficient of residual strength	0.3	0.1	0.1	
Permeability coefficient (k_0)	0.04	0.15	0.12	md
Porosity	0.07	0.17	0.13	
Coupling coefficient (β)	0.01	0.01	0.01	
Coefficient of pore water pressure (α)	0.6	0.6	0.6	

perforation angle on fracture propagation in a layered model. Once the fracturing fluid pressure exceeds the pore pressure and the tensile strength of the reservoir rock, hydraulic fractures initiate and start to propagate. The directions of perforating guns are controlled to make sure the perforation holes lie in the preferred fracture plane, so that the hydraulic fractures can merge with each other as a large single one. However, in shale gas reservoirs, where complex network structures in multiple planes are created, the concept of single-fracture half-length and conductivity are insufficient to describe stimulation performance. Therefore, the concept of SRV is introduced to create complex fracture network and so to maximize the gas recovery. So far, many petroleum engineers and scholars have studied the problem of hydraulic fracture initiation and propagation involving perforation optimization in conventional reservoirs (Van de Ketterij and De Pater 1999; Zhu et al. 2013, 2015; Lu et al. 2015); however, in naturally fractured gas shale formations, few reports have been published about the optimization of perforation to maximize stimulated reservoir volume.

Figure 5 shows the results of progressive fracturing process of fracture network evolution with four perforation angles (which is defined as the angle between perforation direction and σ_H). With the increase in injection pressure, the natural fractures (bedding joints and cross joints) firstly shear stimulation. Hydraulic fracture located besides the wellbore initiates and propagates gradually. The interaction between natural fracture and hydraulic fracture becomes stronger, and SRA increases with the increase in injection fluid. It is noted that hydraulic fracturing effectiveness is the best for perforation angle at 60° . This indicates that for the studied Silurian Longmaxi gas shale formation in this paper, the optimal perforation angle is 60° . The history of injection pressure at the injection wellbore (Fig. 7) shows that with the increase in injected fluid, injection pressure at the wellbore increases until the hydraulic fracture initiation. When the injection pressure reaches the breakdown pressure, the stimulated reservoir area is not the maximum. With the continuous increase in injected fluid, the stimulated reservoir area gets to the maximum at the last injection step, as shown in Fig. 5. Figures 7 and 8 show the qualitative and quantitative comparison results of fracturing network geometry at different perforation angles.

With the RFPA-Flow approach, number of failed elements and the associated energy can be recorded, which can be treated as indicators of microseismic events during fluid injection. The energy and magnitude are related to the strength of failure elements. Figure 9 shows the synthetic microseismic moment magnitudes and distributions for the DFNs with the four studied cases. It is noted that because the natural fractures are subjected to shear failure, the

released energy is very small, so some microseismic actives cannot be recorded during hydraulic fracturing. From the results, number of microseismic events for case "c" is the maximum; however, for case "a" is the minimum; this phenomenon implies that the fracturing effectiveness is the best for case "c". We can also see that for case "c", with the increase in injection rate at each stage, it accumulates the most associated energy with the increase in injection step. Size of circle indicates magnitude of microseismic events, circle diameter for case "c" is the biggest, and this indicates that interaction between HF and DFN is the most obvious. For case "d", number of microseismic events is more than case "a" and case "b", but less than case "c". The complexity of microseismic events was consistent with field observations and suggests an intensive interaction between the created hydraulic fractures and natural fractures. So, it suggests that hydraulic fracturing effectiveness at perforation 60° is the best.

Results of the sensitivity study

As stated above, the model with perforation angle 60° achieves the best SRA; therefore, this section focuses on case 1c to perform parameter sensitivity analysis.

Effect of injection rate

Among many factors that affect the hydraulic fracturing response, the injection rate during hydraulic fracturing is the first critical element to be considered (King 2010; Wang et al. 2015b). The injection rate and injection pressure along with viscosity of the fluid are the operational parameters that can be used to effectively design hydraulic fracturing. Conventional gel fracturing and acidizing operations carried out in the field previously failed to yield the expected productivity in some gas shale formations (Gale and Holder 2008; King 2010). Currently, the general on the mechanism leading to the success of slick-water fracturing in shale gas reservoirs is that a complex fracture network is created by stimulation of pre-existing natural fractures. Therefore, this paper focuses on the study of injection rate to hydraulic fracturing; the slick-water or the low-viscosity stimulation of natural fractures is adopted. Influence of injection rate on the special naturally fractured formation needs to be deeply studied. For the studied Silurian Longmaxi shale gas formation, influence of injection rate on the fracture network evolution is shown in Figs. 10 and 11.

Injection rate as an important operator parameter, the effect of injection rate on hydraulic fracturing treatment depends on the characteristics of formations. As shown in Figs. 10 and 11, it can be seen that for a lower injection

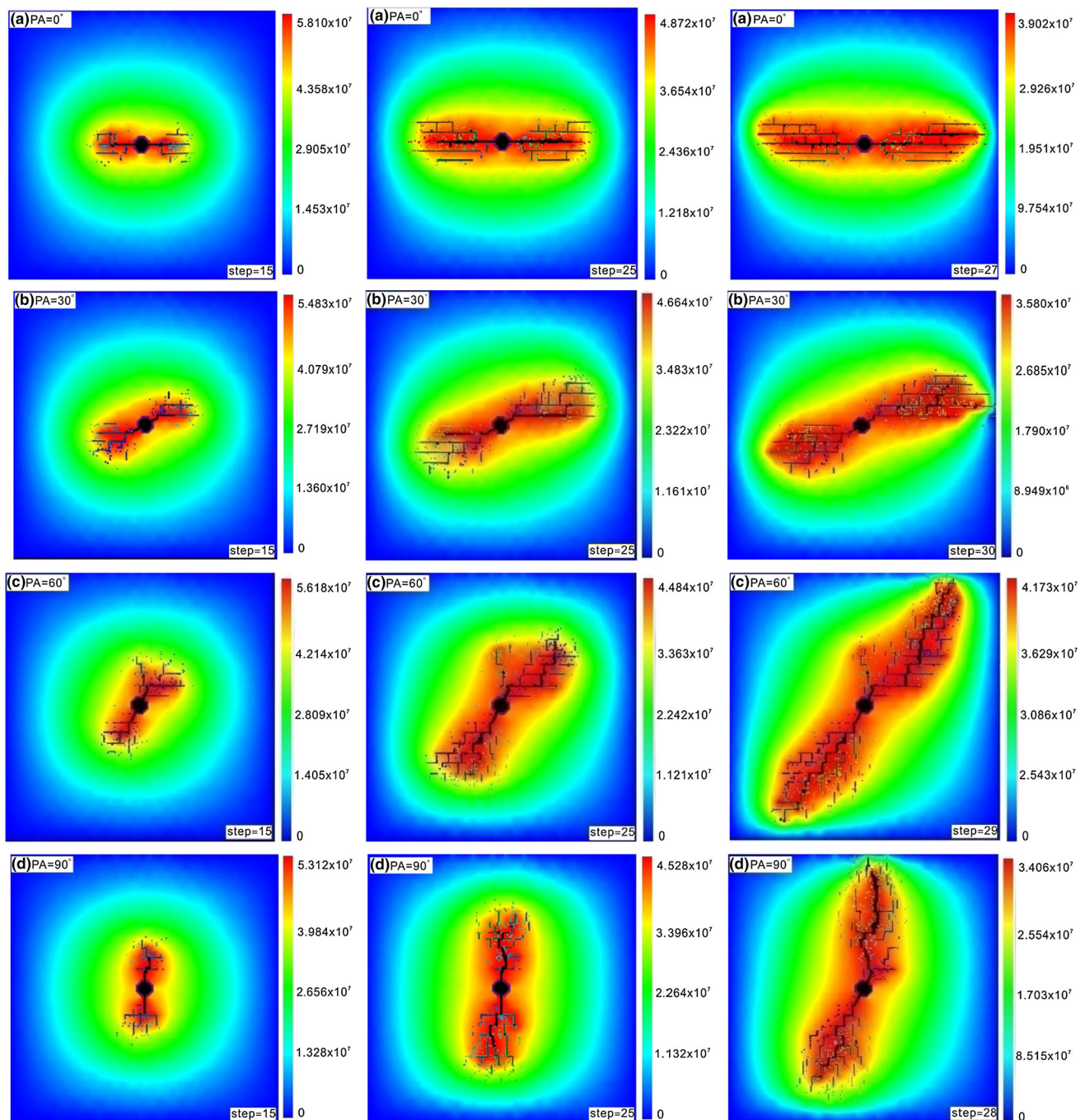


Fig. 5 Fracture network evolution process with perforation angles 0° , 30° , 60° and 90° , respectively. (Color shadow indicates relative magnitude of the pore water pressure field)

rate, the fracturing fluid flows usually along the natural fractures. With higher injection rate, the natural fractures freely deviate from the maximum horizontal stress direction, which becomes very easy for hydraulic fractures. The hydraulic fracture can communicate with natural fractures and greatly increase the SRA. The results indicate that reasonable injection rate design can result in

the maximum stimulated reservoir volume during hydraulic fracturing.

Effect of stress ratio

The index of stress ratio in this paper is defined as the ratio of maximum horizontal stress to vertical stress (σ_H/σ_V).

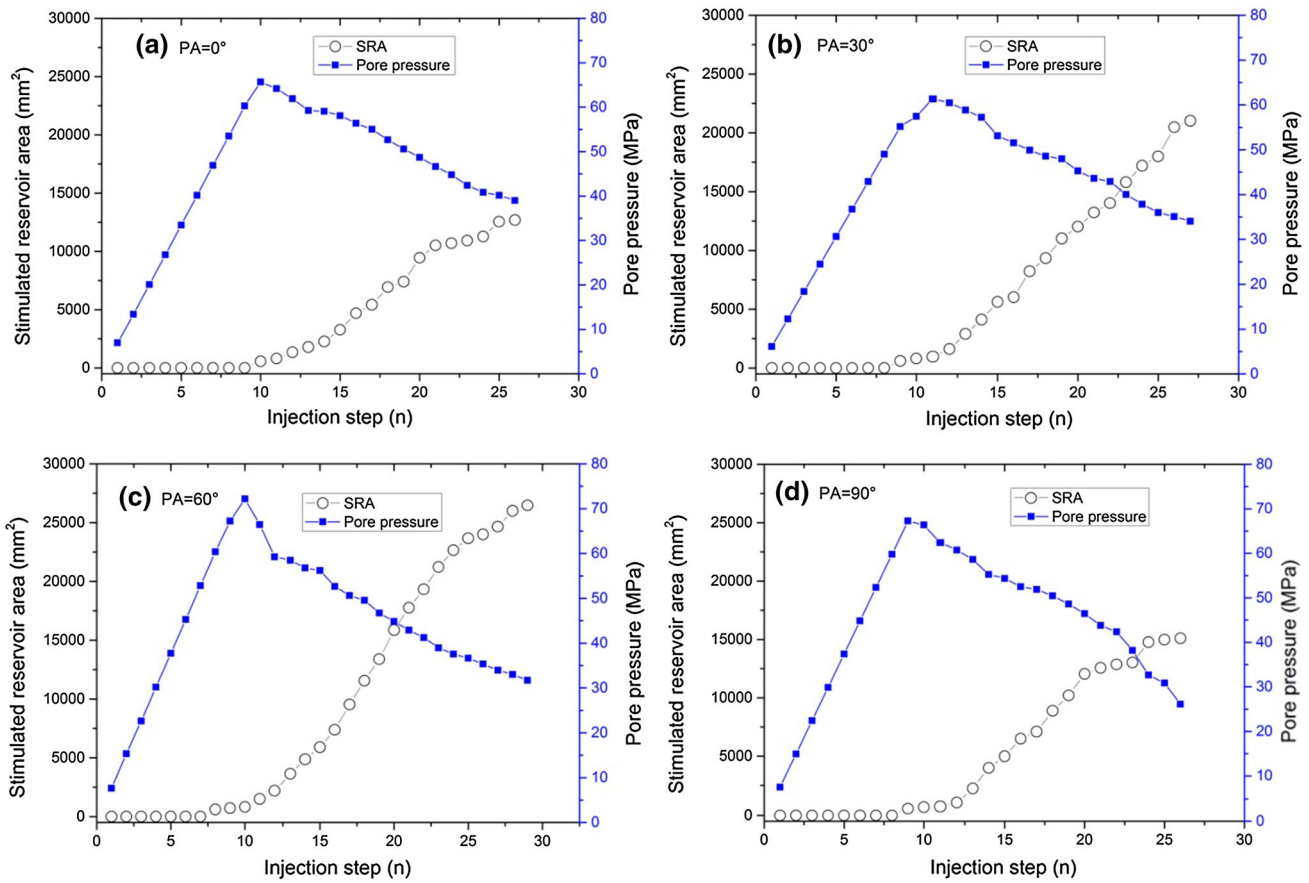


Fig. 6 Variation of fluid pressure and SRA during fluid injection for the different perforation models **a–d** the perforation angle is 0°, 30°, 60°, and 90° respectively

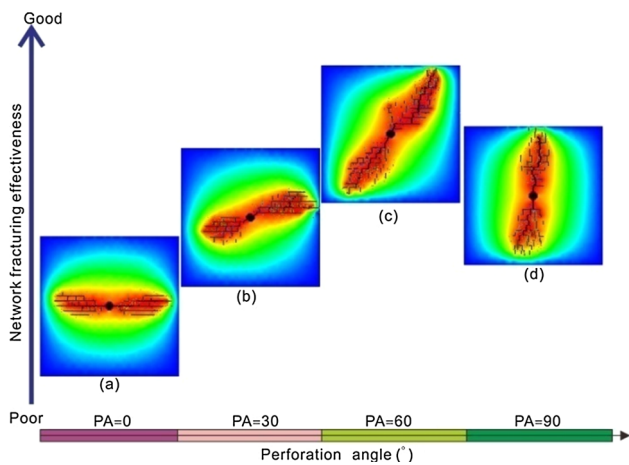


Fig. 7 Geometry of fracturing network for numerical models with different perforation angles

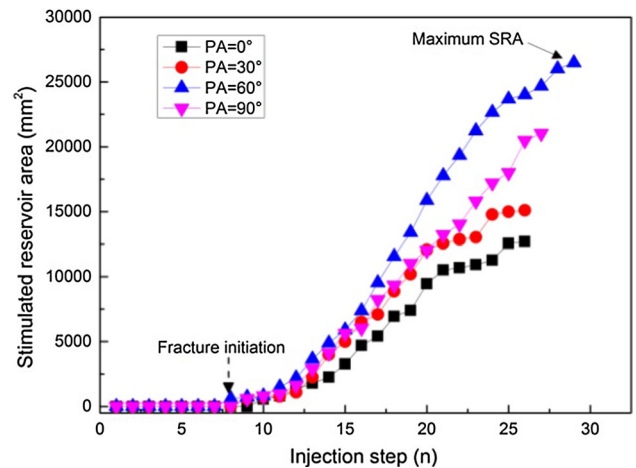


Fig. 8 Relationships between stimulated reservoir area and injection step with perforation angles 0° 30° 60° and 90°, respectively

The in situ stress contrasts obviously have the most significant effect on fracture height growth. The importance of in situ field stress was recognized early in 1961 (Perkins and Kern 1961) and has been extensively studied in

modeling (e.g., Simonson et al. 1978; Voegelé et al. 1983; Palmer and Luiskutty 1985), mineback tests (Warpinski et al. 1982), and numerous laboratory experiments. But few reports about how the stress contrast affects stimulation of

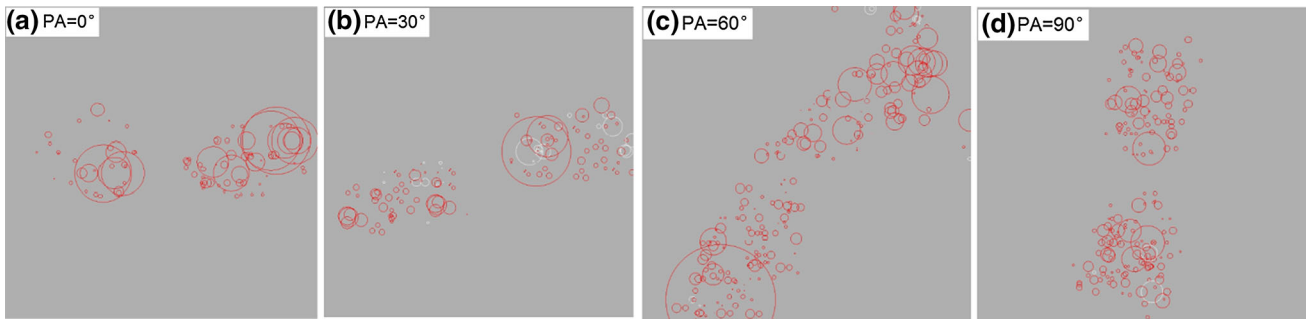


Fig. 9 Synthetic microseismic events at different injection rates for the four studied variable injection rate cases. The synthetic microseismic events are colored by red when elements are tensile failure

and white when compressive shear failure. The size of *circle* indicates magnitude of microseismic events (note that: element whose failure energy is relative small and microseismic sign is not brought out)

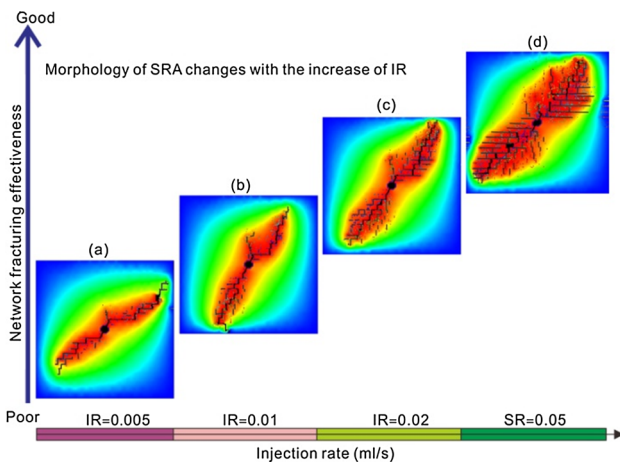


Fig. 10 Geometry of fracturing network with different injection rates (Stimulated reservoir area increases with the increasing injection rate)

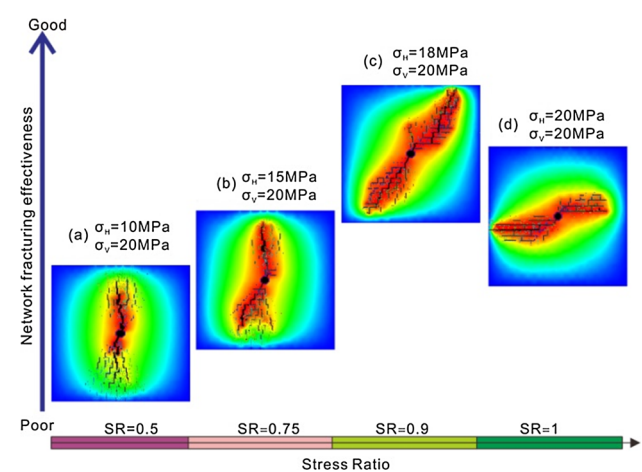


Fig. 12 Geometry of fracturing network for numerical models with different stress ratio

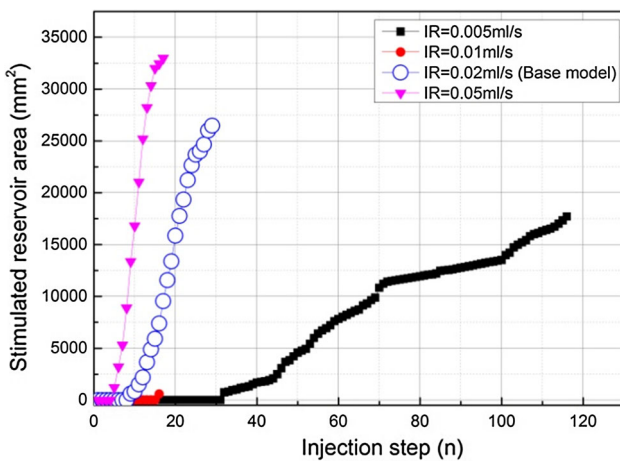


Fig. 11 Relationships between stimulated reservoir area increases and injection step with injection rates 0.005, 0.01, 0.02 and 0.05 ml/s, respectively

natural fractures process were reported. Stress ratio of in situ field also plays an important role in fracturing network evolution process. Therefore, the primary interest in

simulating the sensitivity of stress ratio is to obtain a better understanding of how output is affected by it. Figure 12 presents the results of fracture-stimulated morphology with stress ratio 0.5, 0.75, 0.9 and 1, respectively. It can be seen that, at different stress ratio, the morphology of fracturing network is different. Morphology of fracturing network nearly parallels the vertical stress. For stress ratio equals to 0.5, the value of stimulated reservoir area increases is the minimum; however, for stress ratio equals to 0.9 (base case), the hydraulic fracturing effectiveness is the best. Figure 13 shows the effect of elevated stress ratio and history of quantitative indices.

Effect of IFA on fracturing network evolution

Effect of IFA of cross joint

The objective of this study is to evaluate the effect of the friction angle of cross joints on responses to fluid injection during hydraulic fracturing. For the studied models, as shown in Fig. 14, the propagation of fracturing network is

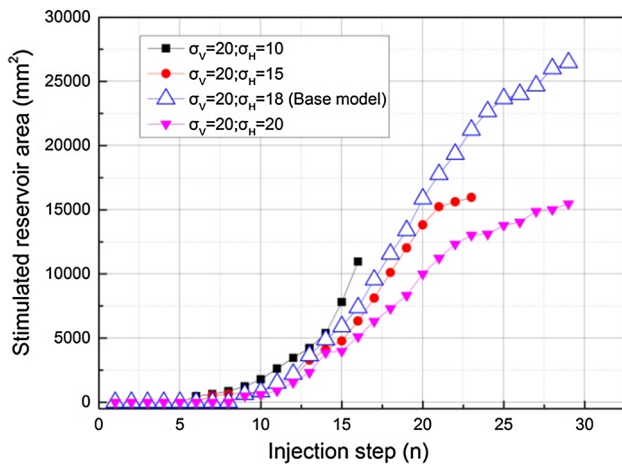


Fig. 13 Relationships between total stimulated area and injection step with stress ratios 0.5, 0.75, 0.9 and 1, respectively

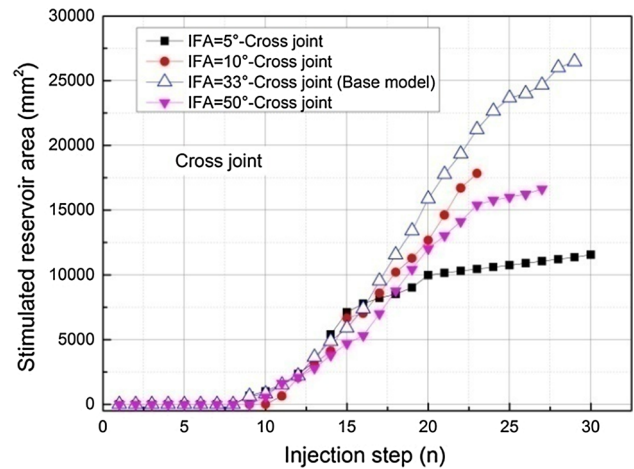


Fig. 15 Relationships between stimulated reservoir area increases and injection step for internal friction angle of cross joint with 5°, 10°, 33° and 50°, respectively

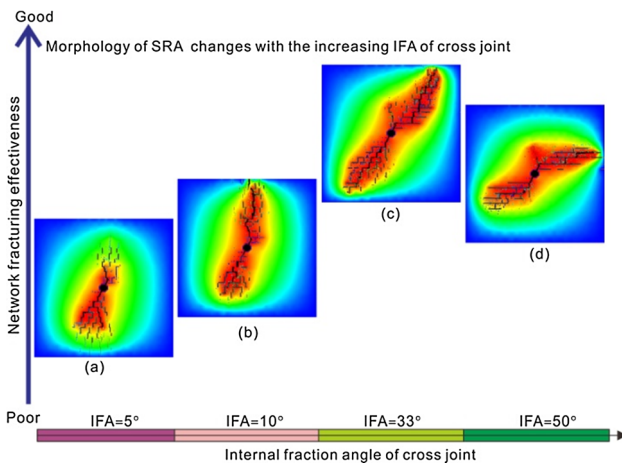


Fig. 14 Geometry of fracturing network for cross joint with different internal fraction angles

different and morphology of fracturing network parallels to vertical stress at lower IFA (5, 10 MPa); it gradually deviates from the direction of vertical stress with the increase in IFA. This phenomenon indicates that the failure of cross joint influences the communication capacity of fracturing network; the internal friction angle is a controlling factor during the evolution of fracturing network. Focusing on shear failure, the common failure criterion is Mohr–Coulomb (Jaeger and Cook 1969). The Mohr–Coulomb criterion can be written as:

$$\tau = S_0 + \mu\sigma \tag{14}$$

where τ is the strength of the material; S_0 is the cohesion of the material; μ is the coefficient of friction within the material and σ is the normal stress acting on the plane of shear failure (Fig. 15).

Shear failure occurs where the shear stress with the material exceeds the shear strength as defined by τ . However, the mechanical behavior of porous media, like shale, is controlled by the effective stress acting on the rock matrix (Terzaghi 1936), where the effective stress can be written in its simplest form as:

$$\sigma' = \sigma - p \tag{15}$$

Combining Eqs. 14 and 15, the shear strength of rock can, at least qualitatively, be given as:

$$\tau = S_0 + \mu(\sigma - p) \tag{16}$$

where: σ is the total normal stress acting on the plane of shear failure; p is pore pressure acting against the total normal stress. Extending the Mohr–Coulomb failure criterion to shale fracture behavior, for cement-filled natural fractures, Eq. 3 becomes:

$$\tau_f = S_f + \mu_f(\sigma_f - p_f) \tag{17}$$

where: τ_f is the shear strength of the cement-filled material; S_f is the cohesion of the cement-filled material; μ_f is the coefficient of friction within the material and σ_f is the normal stress acting on the fracture plane of shear failure; p_f is the pore pressure within the fracture.

Effect of IFA of bedding joint

The internal friction angle of bedding joint is the same to cross joint. Morphology of fracturing network is shown in Fig. 16. As shown, compared with Fig. 14, it can be seen that the morphology of fracturing network is different from the same internal friction angle of cross joint. For IFA = 5° and 50°, propagation of fracturing network is just the opposite. For IFA = 5°, fracturing network

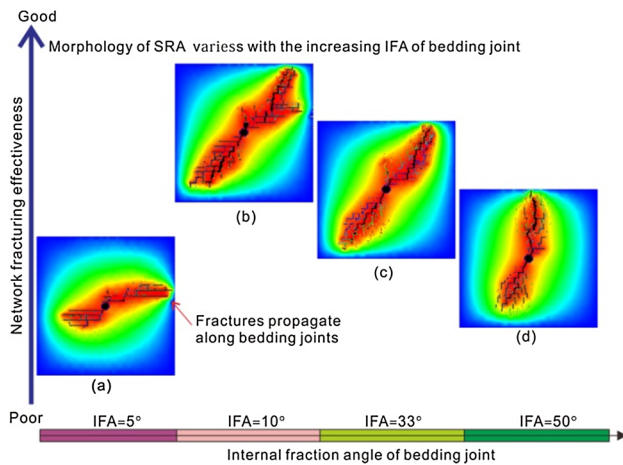


Fig. 16 Geometry of fracturing network for bedding joint with different internal fraction angle

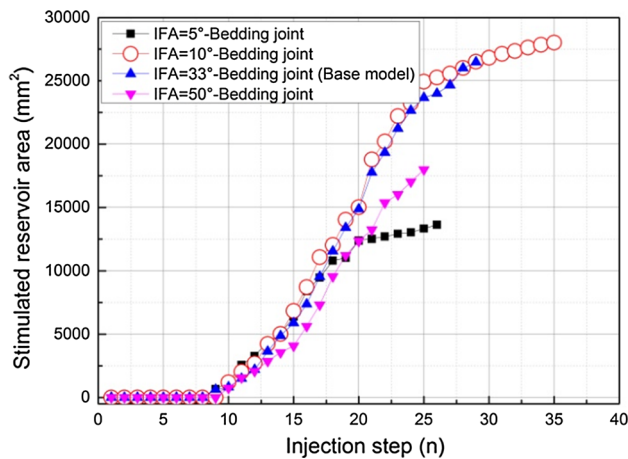


Fig. 17 Relationships between stimulated reservoir area increases and injection step internal for fraction angle of bedding joint with 5°, 10°, 33° and 50°, respectively

propagates along σ_H , not maximum stress (σ_v). This phenomenon can be better interpreted that due to the lower friction angle, fracturing fluid flows along the bedding face and it is difficult to communicate with much more natural fractures. At lower IFA, internal friction angle dominates the evolution of fracturing network. For IFA = 50°, because of the higher internal friction angle of bedding face, bedding joint is difficult to shear stimulation and the in situ stress field dominates the evolution direction of fracturing network (Fig. 17).

Effect of cohesion on fracturing network evolution

Currently, most of the experimental and numerical analysis of hydraulic fracturing has focused on natural fractures with frictional interface. However, core observations form

Longmaxi formation and other plays (e.g., Barnett shale in the Fort Worth Basin) suggest that most natural fractures are largely cemented, i.e., they are sealed pre-existing fractures, and be filled with calcite and quartz cement (Gale et al. 2014). To clarify the effect of cemented natural fractures on hydraulic fracture propagation, Bahorich et al. (2012) performed a series of hydrostone block experiments. They embedded three kinds of inclusions (glass, Berna sandstone and gypsum plaster) into gypsum plaster blocks to represent cemented natural fractures, and studied the influence of sealed fracture. However, for their experiment, the natural fracture is simplified as a single plane, which cannot reflect the complex natural fracture system in shale formation. Also, the cohesion of cemented material is hard to control. For this complicated problem, numerical simulation techniques may provide a feasible alternative solution. This section, the effect of cohesion of cross joint and bedding joint is studied, respectively.

Effect of cohesion of cross joint

The influence of cohesion of cross joint on fracturing network is discussed. Figures 18 and 19 are the qualitative and quantitative of simulation results when the fractures are in different cohesion. As shown in Fig. 18, different fracturing network morphology was observed, at lower cohesion (3 MPa), and it propagates along the direction of vertical stress (Fig. 18a); with the increase in cohesion, at cohesion of 9 MPa, the hydraulic fracture can communicate with natural fractures and greatly increase the stimulated reservoir area increases. At high cohesion (15, 20 MPa), because of the relative lower shear strength of bedding face (9 MPa), bedding joints are easy to be stimulated and fracturing fluid flows along the bedding face,

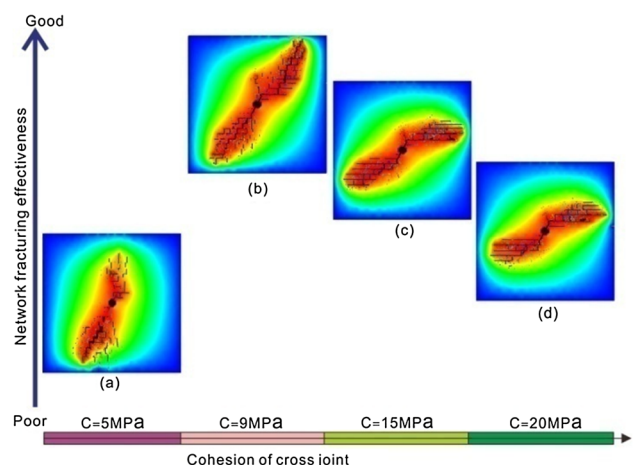


Fig. 18 Geometry of fracturing network for cross joint with different cohesion

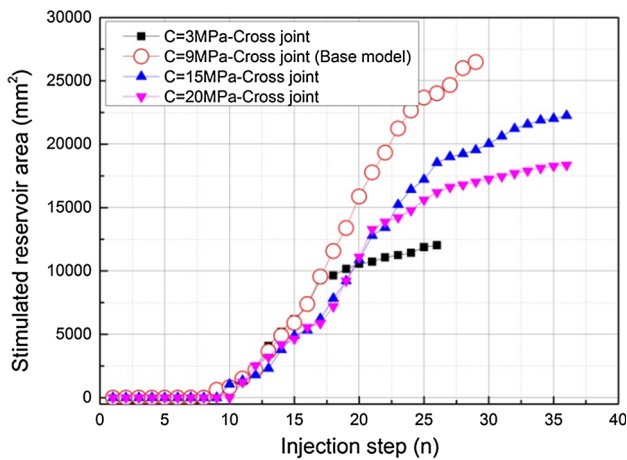


Fig. 19 Relationships between stimulated reservoir area and injection step for cohesion of cross joint with 3, 9, 15 and 20 MPa, respectively

resulting in decrease in stimulated reservoir area increases. This result further implies that it is not the case that the lower the cohesion of natural fractures, the better stimulated reservoir area can be obtained. Observing the simulation result in Fig. 18, at the cohesion of 9 and 15 MPa, the hydraulic fracturing effectiveness is better than other two circumstances. Figure 19 shows the effect of elevated cohesion and history of quantitative indices. When the cohesion equals to 9 MPa, in this case, the hydraulic fracturing effectiveness is the best. This result can be better interpreted that at the same boundary conditions, the evolution of fracturing network is determined by both the cross joint and bedding joint.

Effect of cohesion of bedding joint

Figures 20 and 21 are the qualitative and quantitative of simulation results when the bedding joints are in different cohesion. Morphology of fracturing network is different from Fig. 18, at the same cohesion. This suggests that impact of natural fracture on SRA is related to dip direction of natural fractures. As shown in Fig. 20, the morphology of fracturing network is different from Fig. 18. With lower cohesion (5 MPa), natural bedding faces easily shear stimulation. The injected fluid flows along the bedding faces, and it is disadvantageous to achieve complex fracturing network. In this case, the weak face plays a dominate role in controlling the evolution of fracturing network. With higher cohesion (20 MPa), because of the strong cemented property, bedding joint is difficult to reopen; at this condition, the in situ stress field plays a dominate role in controlling the evolution of fracturing network. Figure 21 shows the relationships between stimulated reservoir area and injection step with different cohesion of bedding joint and history of quantitative indices. With the increase in cohesion,

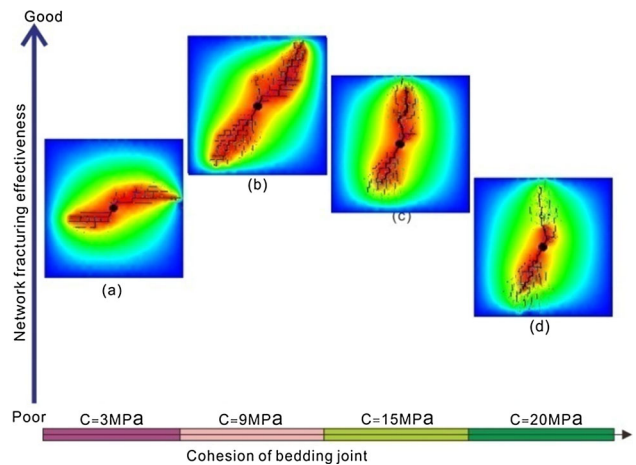


Fig. 20 Geometry of fracturing network for cross joint with different cohesion

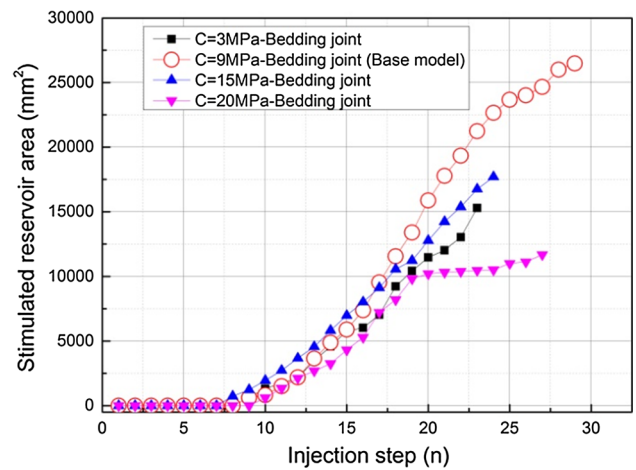


Fig. 21 Relationships between stimulated reservoir area and injection step for cohesion of bedding joint with 3, 9, 15 and 20 MPa, respectively

stimulated reservoir area firstly increases and then decreases. There exists an optimal value of cohesion making the maximum of stimulated reservoir area.

By analyzing the results in Figs. 14, 16, 18 and 20, we can draw the conclusion that propagation of fracturing network is not always oriented to maximum principle stress. Propagation of fracturing network is also strongly affected by cohesive and frictional strength of natural fractures.

Conclusions

Microseismic data, logging image and coring studied suggest that existence of natural fractures result in the complex fracturing network in naturally fractured shale reservoirs. However, direct observations of subsurface

morphology of fracturing network are incomplete and difficult; we adopt proper numerical modeling based on realistic assumptions to help us grasp the formation and evolution of fracturing network. This designed numerical work cannot be substituted for the hydraulic fracturing design tools, but it can help us to understand and grasp the effects of hydraulic fracturing with some important geomechanical parameters and the operational parameters.

From the sensitivity study in this paper, several important results can be drawn as follows:

1. Perforation angle is a critical completion parameter affecting the stimulated reservoir volume. In the paper, for the studied Silurian Longmaxi shale formation southeast of Sichuan Basin, China, the optimal perforation angle is 60°. It is really needed to note that optimal perforation angle is related to development characteristics of natural fractures.
2. Injection rate plays a critical role in distributing the fluid between the hydraulic fractures and the natural fractures. It has different impacts on fracture complexity during hydraulic fracturing. At lower injection rate, the fracturing fluid flows usually along the cross fractures and bedding faces and the hydraulic fracture effectiveness is poor. With the increase in injection rate in a certain range, hydraulic fracture can communicate with natural fractures and greatly increase the stimulated reservoir area.
3. Fracturing network is strongly related to the morphology of natural fractures. Fracture complexity is thought to be enhanced when pre-existing fractures are oriented at an angle to the maximum stress direction, in this case, because these combinations of stress and natural fractures allow fractures to be stimulated in multiple orientations.
4. Effects of mechanical properties of bedding joint and cross joint on fracturing network are not the same. It is not the case that the lower mechanical strength of natural fracture and the good fracturing effectiveness can be obtained. There exists an optimal value of internal friction angle and cohesion leading to the maximum of stimulated reservoir area.
5. The mechanical properties of fracture cement-filled material affect the morphology characteristics of fracturing network. The shear of fractures is linked to the microseismic events; the shear region within the natural fracture system is strongly related to the geomechanical parameters of fractures in shales.

Acknowledgments We thank the editors and the anonymous reviewers for their helpful and constructive suggestions and comments. This work was supported by the National Natural Science Foundation of China (Grants Nos. 41330643, 41227901, 41502294), Beijing National Science Foundation of China (Grants Nos.

8164070), China Postdoctoral Science Foundation Funded Project (Grants Nos. 2015M571118), and the Strategic Priority Research Program of the Chinese Academy of Sciences (Grants Nos. XDB10030000, XDB10030300, and XDB10050400).

References

- Al-Busaidi A, Hazzard JF, Young RP (2005) Distinct element modeling of hydraulically fractured Lac du Bonnet granite. *J Geophys Res Solid Earth* 110(B6):1–14
- Baecher GB, Lanne NA, Einstein HH (1978) Statistical description of rock properties and sampling. In: *Proceedings of the 18th U.S. symposium on rock mechanics* vol 5, pp 1–8
- Bahorich B, Olson JE, Holder J (2012) Examining the effect of cemented natural fractures on hydraulic fracture propagation in hydrostone block experiments. *SPE* 160197
- Bredheoht JD, Wolff RG, Keys WS, Shuter E (1976) Hydraulic fracturing to determine the regional in situ stress field, Piceance Basin, Colorado. *Geo Soc Am Bull* 87(2):250–258
- Britt LK, Schoeffler J (2009) The geomechanics of a shale play: what makes a shale prospective! In: *SPE 125525*, presented at the 2009 SPE Eastern regional Meeting, Charleston, West Virginia; September 23–25
- Bruno MS, Nakagawa FM (1991) Pore pressure influence on tensile fracture propagation in sedimentary rock. *Int J Rock Mech Mining Sci* 28(4):261–273
- Cacas MC, Ledoux E, Marsily GD, Barbreau A, Calmels P, Gaillard B (1990) Margritta R (1990) Modeling fracture flow with a stochastic discrete fracture network: calibration and validation: 2 the transport model. *Water Resour Res* 26(3):491–500. doi:10.1029/WR026i003p00491
- Cipolla CL, Lolon EP, Erdie JC (2009a) Modeling well performance in shale-gas reservoirs. Presented at the SPE/EAGE Reservoir Characterization and Simulation Conference held in Abu Dhabi, UAE, October 19–21
- Cipolla CL, Lolon EP, Mayerhofer MJ (2009b) Reservoir modeling and production evaluation in shale-gas reservoirs. Presented at the international petroleum technology conference held in Doha, Qatar, 7–9 December
- Clifton RJ, ABOU-sayed AS (1979) On the computation of the three-dimensional geometry of hydraulic fractures. *SPE*8943
- Dezayes C, Genter A, Valley B (2010) Structure of the low permeable naturally fractured geothermal reservoir at Soultz. *C R Geosci* 342(7–8):517–530. doi:10.1016/j.crte.2009.10.002
- EI Rabaa W (1989) Experimental study of hydraulic fracture geometry initiated from horizontal wells. *SPE annual technical conference and exhibition, Society of Petroleum Engineers, San Antonio, Texas*
- EngelderT, Lash GG (2008) Marcellus Shale Play's vast resource potential creating stir in Appalachia. *The American Oil and Gas Reporter*, May
- Fu P, Johnson SM, Carrigan CR (2013) An explicitly coupled hydrogeomechanical model for simulating hydraulic fracturing in arbitrary discrete fracture networks. *Int J Numer Anal* 37(14):2278–2300
- Gale JFW, Holder J (2008) Natural fractures in the Barnett shale: constraints on spatial organization and tensile strength with implications for hydraulic fracture treatment in shale-gas reservoirs: the 42nd U. S. Rock Mechanics Symposium (USRMS),-San Francisco, CA, June 29–July 2
- Gale JFW, Stephen EL, Olson JE, Eichhubl P, Fall A (2014) Natural fractures in shale: a review and new observations. *AAPG Bull* 11(98):2165–2216

- Haimson B (1968) Hydraulic fracturing in porous and nonporous rock and its potential for determining in-situ stresses at great depth. Ph.D. Dissertation Minnesota University, Minneapolis, MN, United States
- Hallam SD, Last NC (1991) Geometry of hydraulic fractures from modestly deviated wellbore. *J Pet Technol* 43(6):742–748
- Heng S, Guo YT, Yang CH (2015) Experimental and theoretical study of the anisotropic properties of shale. *Int J Rock Mech Min Sci* 74:58–68 (in Chinese)
- House L (1987) Locating microearthquakes induced by hydraulic fracturing in crystalline rock. *Geophys Res Lett* 14(9):919–921
- Jaeger JC, Cook NGW (1969) *Fundamentals of rock mechanics*, 3rd edn. Wiley, New York
- Jeffrey RG, Zhang X, Bungler AP (2010) Hydraulic fracturing of naturally fractured reservoirs. In: *Proceedings of the 35th workshop on geothermal reservoir engineering*, Stanford, California, USA, 1–3, February
- King GE (1989) Perforating the horizontal well. *J Pet Technol* 41(7):671–672
- King GE (2010) Thirty years of gas shale fracturing: what have we learned? Paper SPE 133456 presented at the SPE annual technical conference and exhibition, Florence, Italy, 19–22 September
- Kresse O, Cohen C, Weng X, Gu HG, Wu RT (2011) Numerical modeling of hydraulic fracturing in naturally fractured formations. Paper ARMA 11-363 presented at the 45th US Rock Mechanics Symposium, San Francisco, California, USA, 26–29 June
- Li Z, Jia CG, Yang CH (2015) Propagation of hydraulic fissures and bedding planes in hydraulic fracturing of shale. *Chin J Rock Mech Eng* 34(1):12–20 (in Chinese)
- Li L, Meng Q, Wang S, Li G, Tang CA (2013) A numerical investigation of the hydraulic fracturing behaviour of conglomerate in Glutenite formation. *Acta Geotechnica* 8(6):597–618
- Liu GH, Pang F, Chen ZX (2000) Fracture simulation tests. *J China Univ Pet* 24(5):23–31 (in Chinese)
- Lockner D, Byerlee JD (1977) Hydrofracture in Weber Sandstone at high confining pressure and differential stress. *J Geophys Res* 82(14):2018–2026. doi:10.1029/JB082i014p02018
- Lu C, Guo JC, Liu YX, Yin J, Deng Y, Lu QL, Zhao X (2015) Perforation spacing optimization for multi-stage hydraulic fracturing in Xujiahe formation: a tight sandstone formation in Sichuan Basin of China. *Environ Earth Sci* 73:5843–5854
- Mandal N, Deb SK, Khan D (1994) Evidence for a non-linear relationship between fracture spacing and layer thickness. *J Struct Geol* 16(9):1275–1281
- Mayerhofer MJ, Lolon EP, Warpinski NR, Cipolla CL, Walser D, Rightmire CM (2008) What is stimulated rock volume (SRV)? In: SPE 119890, presented at the 2008 SPE shale gas production conference, Fort Worth, Texas; November 16–18
- McCabe WJ, Barry BJ, Manning MR (1983) Radioactive tracers in geothermal underground water flow studies. *Geothermics* 12(2–3):83–110. doi:10.1016/0375-6505(83)90020-2
- McClure M, Horne RN (2013) *Discrete fracture network modeling of hydraulic stimulation: Coupling flow and geomechanics*. Springer Science & Business Media, 2013
- Men XX, Tang CA, Wang SY, Li YP, Yang T, Ma TH (2013) Numerical simulation of hydraulic fracturing in heterogeneous rock: the effect of perforation angles and bedding plane on hydraulic fractures evolutions. ISRM International conference for effective and sustainable hydraulic fracturing. International Society for Rock Mechanics
- Meyer BR, Bazan LW (2011) A discrete fracture network model for hydraulically induced fractures –theory, parametric and case studies. Paper SPE 140514 presented at the SPE hydraulic fracturing technology conference and exhibition, The Woodlands, Texas, USA, 24–26 January
- Miller C, Waters G, Rylander E (2011) Evaluation of production log data from horizontal wells drilled in organic shales, SPE 144326. Paper presented at the North American unconventional gas conference and exhibition, The Woodlands, Texas, USA. doi:10.2118/144326
- Nagel NB, Sanchez-Nagel MA, Zhang F, Garica BL (2013) coupled numerical evaluations of the geomechanical interactions between a hydraulic fracture stimulation and a natural fracture system in shale formations. *Rock Mech Rock Eng* 46(3):581–609
- Nassir M, Settari A, Wan R (2010) Modeling shear dominated hydraulic fracturing as a coupled fluid-solid interaction. Paper SPE 131736 presented at the international oil and gas conference and exhibition, Beijing, China, 8–10 June
- Noghabai K (1999) Discrete versus smeared versus element-embedded crack models on ring problem. *J Eng Mech* 125(3):307–315
- Olson JE (2003) Sublinear scaling of fracture aperture versus length: an exception to the rule? *J Geophys Res* 108:1–11
- Olson JE (2004) Predicting fracture swarms—the influence of subcritical crack growth and the crack-tip process zone on joint spacing in rock. *Geol Soc* 231:73–88
- Palmer I, Luiskutty CT (1985) A model of the hydraulic fracturing process for elongated vertical fractures and comparisons of results with other models. Paper SPE 13864 presented at the SPE/DOE low permeability gas reservoirs symposium, Denver, Colorado, 19–22 May
- Palmer I, Moschovidis Z (2010) New method to diagnose and improve shale gas completions. Paper SPE 134669 presented at the SPE annual technical conference and exhibition, Florence, Italy, 19–22 September
- Pearson CM, Bond AJ, Eck ME, Schmlidt JH (1992) Results of stress oriented and aligned perforating in fracturing deviated wells. *J Pet Technol* 44(1):10–18
- Perkins TK, Kern LR (1961) Widths of hydraulic fractures. *JPT* 13:937–949
- Rahman MM, Rahman SS (2013) Studies of hydraulic fracture-propagation behavior in presence of natural fractures: fully coupled fractured-reservoir modeling in poroelastic environments. *Int J Geomech* 13(6):809–826
- Rutqvist J, Wu YS, Tsang F, Bodvarsson G (2002) A modeling approach for analysis of coupled multiphase fluid flow, heat transfer, and deformation in fractured porous rock. *Int J Rock Mech Min* 39(4):429–442
- Sagy A, Reches Z (2004) Joint intensity in layered rocks: the unsaturated, saturated, supersaturated, and clustered classes. Institute of Earth Sciences, Hebrew University
- Simonson ER, Abou-Sayed AS, Clifton JJ (1978) Containment of massive hydraulic fractures. *SPE J* 18:27–32
- Tang CA, Tham LG, Lee PKK (2002) Coupled analysis of flow, stress and damage (FSD) in rock failure. *Int J Rock Mech Min Sci* 39:477–489
- Terzaghi K (1936) The shearing resistance of saturated soils and the angle between the planes of shear. International conference on soil mechanics and foundation engineering. Harvard University Press, Cambridge, pp 54–56
- Thallak S, Rothenbury L, Dusseault M (1991) Simulation of multiple hydraulic fractures in a discrete element system. In: Roegiers JC (ed) *Rock mechanics as a multidisciplinary science*, Proceedings of the 32nd US Symposium. Balkema, Rotterdam, pp 271–280
- Van de Ketterij RG, De Pater CJ (1999) Impact of perforations on hydraulic fracture tortuosity. *SPE Prod Facil* 14(2):131–138
- Voegelé MD, Abou-Sayed AS, Jones AH (1983) Optimization of stimulation design through the use of in-situ stress determination. *JPT* 35:1071–1081
- Wang Y, Li X, Zhou RQ, Tang CA (2015a) Numerical evaluation of the shear stimulation effect in naturally fractured formations. *Science China: Earth Sciences*, doi: 10.1007/s11430-015-5204-5

- Wang Y, Li X, Zhou RQ, Zheng B, Zhang B, Wu YF (2015b) Numerical evaluation of the effect of fracture network connectivity in naturally fractured shale based on FSD model. *Science China: Earth Sciences*, doi: [10.1007/s11430-015-5164-9](https://doi.org/10.1007/s11430-015-5164-9)
- Wang Y, Li X, Zhao ZH, Zhou RQ, Zhang B (2016) Contributions of non-tectonic micro-fractures to hydraulic fracturing: a numerical investigation based on FSD model. *Sci China Earth Sci*. doi:[10.1007/s11430-015-5232-1](https://doi.org/10.1007/s11430-015-5232-1)
- Warpinski NR, Fnley SJ, Vollendorf WC (1982) The interface test series: an in situ study of factors affecting the containment of hydraulic fractures. Sandia National Laboratories Report, SAND, pp 2381–2408
- Yang TH, Tham LG, Tang CA, Liang ZZ, Tsui Y (2004) Influence of heterogeneity of mechanical properties on hydraulic fracturing in permeable rocks. *Rock Mech Rock Eng* 37(4):251–275
- Zhu HY, Deng JG, Chen ZJ (2013) Perforation optimization of hydraulic fracturing of oil and gas well. *Geomech Eng* 5(5):463–483
- Zhu HY, Deng JG, Jin XC (2015) Hydraulic fracture initiation and propagation from wellbore with oriented perforation. *Rock Mech Rock Eng* 48:585–601
- Zoback MD, Rummel F, Jung R (1997) Laboratory hydraulic fracturing experiments in intact and pre-fractured rock. *Int J Rock Mech Min Sci Geomech Abst Pergamon* 14(2):49–58